https://doi.org/10.5194/egusphere-2026-6766
Preprint. Discussion started: 19 November 2026
© Author(s) 2026. CC BY 4.0 License.

Measurement Report: Seasonal and Vertical Variations in $PM_{2.5}$ Water-Soluble Matter Hygroscopicity at Mt. Hua, Central China: Insights from Inorganic and Organic Fractions

Xin Wang[1], Yukun Chen[2], Jialin Wu[3], Biao Li[4], Yali Liu[5,6], Yifan Zhang[5,6], Yue Cao[5,6], Minxia Shen[5,6], Wenting Dai[5,7], Lu Li[5], Xiao Guo[5], Jianjun Li[5,7*], Fobang Liu[3], Yueshe Wang[4]

[1]School of Chemistry, Xi'an Jiaotong University, Xi'an 710049, China
[2]National Key Laboratory of Aerospace Chemical Power, Hubei Institute of Aerospace Chemo-technology, Xiangyang 441000, China
[3]Department of Environmental Science and Engineering, School of Energy and Power Engineering, Xi'an Jiaotong University, Xi'an 710049, China
[4]State Key Laboratory of Multiphase Flow in Power Engineering, Xi'an Jiaotong University, Xi'an 710049, China
[5]State Key Laboratory of Loess Science, Institute of Earth Environment, Chinese Academy of Sciences, Xi'an 710061, China
[6]Xi'an Institute for Innovative Earth Environment Research, Xi'an, China
[7]National Observation and Research Station of Regional Ecological Environment Change and Comprehensive Management in the Guanzhong Plain, Xi'an, China

[*]*Correspondence to*: Jianjun Li (lijj@ieecas.cn)

Abstract. Aerosol hygroscopicity plays an important role in atmospheric water uptake and is strongly influenced by chemical composition and atmospheric processing. Here, we investigated seasonal and vertical variations in the composition and hygroscopicity of $PM_{2.5}$ water-soluble matter (WSM) at the summit and foothill of Mt. Hua, central China. WSM hygroscopicity was significantly higher in summer than in winter and at the summit than at the foothill. The hygroscopicity parameter (κ_{WSM}) averaged 0.30 ± 0.05 and 0.18 ± 0.05 at the summit and 0.24 ± 0.10 and 0.16 ± 0.03 at the foothill in summer and winter, respectively. These variations were accompanied by seasonal and vertical differences in chemical composition and air-mass transport. Summer aerosols had a greater relative contribution of sulfate, whereas biomass-burning- and mineral-related components became more important in winter. Correlations between WSM hygroscopicity and individual components generally weakened when analyzed separately by season, suggesting substantial seasonal covariation between composition and hygroscopicity. Separation of WSM into predominantly inorganic (WSIM) and organic (WSOM) fractions showed that WSIM was substantially more hygroscopic and more variable than WSOM. However, seasonal changes in bulk WSM hygroscopicity did not simply follow those of either fraction. Zdanovskii–Stokes–Robinson calculations better reproduced WSIM hygroscopicity when K^+-,

https://doi.org/10.5194/egusphere-2026-6766
Preprint. Discussion started: 19 November 2026
© Author(s) 2026. CC BY 4.0 License.

Ca^{2+}-, and Mg^{2+}-containing species were included, particularly in winter. These results suggest that WSM hygroscopicity reflects the combined effects of air-mass transport, organic–inorganic partitioning, and detailed chemical composition rather than individual components alone.

1. Introduction

Atmospheric aerosol hygroscopicity describes the ability of particles to take up water and is closely related to their size, phase state, optical properties, and cloud condensation nuclei (CCN) activity. (Petters and Kreidenweis, 2007; Pöschl, 2005). Hygroscopicity is strongly dependent on chemical composition. Inorganic salts such as ammonium sulfate and ammonium nitrate generally exhibit substantial water uptake, whereas organic aerosol shows a much wider range of hygroscopic behavior depending on its sources, composition, and atmospheric aging (Saxena et al., 1995; Duplissy et al., 2011; Swietlicki et al., 2008). For ambient aerosols containing complex mixtures of inorganic and organic species, water uptake therefore depends on both their relative abundance and hygroscopic properties. The complex and variable composition of ambient aerosols can therefore result in substantial spatial and temporal variability in aerosol hygroscopicity, with water uptake reflecting the combined effects of chemical composition, mixing state, sources, and atmospheric processing (Swietlicki et al., 2008; Peng et al., 2020).

Water-soluble matter (WSM) is particularly relevant to aerosol hygroscopic growth because it contains both highly hygroscopic inorganic salts and chemically diverse water-soluble organic matter (WSOM). Previous studies have shown that WSM hygroscopicity varies considerably with the relative contributions of inorganic and organic material (Gysel et al., 2004; Boreddy and Kawamura, 2016). However, changes in bulk WSM hygroscopicity may arise not only from changes in the inorganic-to-organic ratio but also from variations in the hygroscopic properties of the individual fractions. Even within the inorganic fraction, water uptake depends on ionic composition and the chemical forms in which the ions are present. Hygroscopicity closure based on the Zdanovskii–Stokes–Robinson (ZSR) mixing rule has been widely used to relate chemical composition to aerosol water uptake, but discrepancies between calculated and measured hygroscopicity have also been reported (Healy et al., 2014; Swietlicki et al., 2008). Separating water-soluble inorganic and organic fractions may therefore provide a useful approach for examining their respective contributions to bulk WSM hygroscopicity.

https://doi.org/10.5194/egusphere-2026-6766
Preprint. Discussion started: 19 November 2026
© Author(s) 2026. CC BY 4.0 License.

Mountain environments provide an opportunity to examine these compositional effects under contrasting source and transport conditions. Mountain aerosols can be influenced by boundary-layer emissions, regional transport, and air masses with different degrees of atmospheric processing, and their relative importance changes with season and meteorological conditions (Okamoto and Tanimoto, 2016; Collaud Coen et al., 2018). Consequently, substantial variations in aerosol composition and hygroscopicity have been observed at high-altitude sites, often in association with changes in air-mass origin and secondary aerosol formation (Sjogren et al., 2008; Holmgren et al., 2014). Simultaneous measurements at a mountain summit and nearby foothill can provide further information on how differences in source influence and transport are reflected in aerosol composition and hygroscopicity, yet such measurements across different seasons remain relatively limited.

Mt. Hua, located on the southeastern edge of the Guanzhong Plain in central China, is influenced by both emissions from surrounding populated regions and regional transport. Previous studies have reported clear summit–foothill differences in aerosol composition and demonstrated the importance of mountain–valley circulation and regional transport in determining the chemical characteristics of aerosols reaching the mountain atmosphere (Li et al., 2011; Feng et al., 2023; Chen et al., 2023). Recent in situ measurements using a hygroscopic tandem differential mobility analyzer (H-TDMA) at the summit further showed variations in aerosol hygroscopicity associated with particle size and air-mass origin (Shi et al., 2026). However, the seasonal variation in aerosol hygroscopicity and its vertical contrast between the summit and foothill remain less well characterized, particularly in relation to changes in water-soluble composition and transport. The contributions of water-soluble inorganic and organic fractions to these variations are also poorly constrained.

In this study, $PM_{2.5}$ samples were collected simultaneously at the summit and foothill of Mt. Hua during summer and winter to investigate the seasonal and vertical variations in the chemical composition and hygroscopicity of WSM. Backward trajectory and potential source contribution function (PSCF) analyses were used to examine how differences between seasons and elevations were associated with air-mass transport. To further investigate the compositional factors affecting WSM hygroscopicity, WSM was separated into predominantly water-soluble inorganic and organic fractions, and the measured hygroscopicity of the inorganic fraction was compared with ZSR calculations based on ionic composition.

https://doi.org/10.5194/egusphere-2026-6766
Preprint. Discussion started: 19 November 2026
© Author(s) 2026. CC BY 4.0 License.

2. Methods

2.1 Sampling sites and aerosol collection

$PM_{2.5}$ samples were collected simultaneously at a mountain summit and a foothill site on Mt. Hua (34.48° N, 110.09° E); the summit site (West Peak) is at 2060 m a.s.l., while the foot site is at 385 m a.s.l., providing an elevation difference of approximately 1675 m (Figure S1). Sampling campaigns were conducted during the summer (July 30–August 31, 2020) and winter (December 16, 2020–January 12, 2021). $PM_{2.5}$ samples were collected on pre-baked (450 ºC, 6 h) quartz fiber filters using median-volume samplers operating at 100 L min^{-1} for 11 hours (daytime: 8:00–19:00; nighttime: 20:00–7:00). Filter-based $PM_{2.5}$ mass was determined gravimetrically using an electronic microbalance with a sensitivity of ±1 μg (Mettle M3, Switzerland). Before weighing, the sample filters were equilibrated at 20–23°C and at a relative humidity of 35%–45% for 24 h. Field blanks were collected throughout the campaigns following the same handling procedures as the ambient samples. Upon collection, filters were wrapped in pre-baked aluminum foil and stored at -20 ºC until analysis.

Meteorological parameters, including temperature, relative humidity (RH), wind speed, wind direction, and visibility, were obtained from the Huashan Meteorological Observatory at the summit and the Huayin Meteorological Station at the foothill.

2.2 Chemical analysis

Water-soluble inorganic ions and water-soluble organic carbon (WSOC) were determined following the procedures described in (Li et al., 2020; Zhang et al., 2011). Briefly, portions of the $PM_{2.5}$ filter samples were extracted with ultrapure water by ultrasonication in an ice bath for 30 min. The extracts were filtered before analysis. Major inorganic ions (SO_4^{2-}, NO_3^-, Cl^-, NH_4^+, Ca^{2+}, K^+, Na^+, and Mg^{2+}) were measured by ion chromatography (Metrohm 940), while WSOC was determined using a total organic carbon analyzer (Shimadzu TOC-L CPH). Water-soluble organic matter (WSOM) concentrations were estimated by multiplying WSOC concentrations by a factor of 2.1 (Boreddy et al., 2016; Chen et al., 2021).

2.3 Hygroscopicity measurements

2.3.1 Hygroscopicity measurements of bulk water-soluble matter

https://doi.org/10.5194/egusphere-2026-6766
Preprint. Discussion started: 19 November 2026
© Author(s) 2026. CC BY 4.0 License.

The hygroscopicity of bulk water-soluble matter (WSM) was measured using a hygroscopic tandem differential mobility analyzer (H-TDMA, MSP 1040X). The instrument configuration and measurement procedures have been described previously (Chen et al., 2021; Wang et al., 2026). Briefly, aqueous extracts were atomized, and the resulting particles were dried to a relative humidity (RH) below 5%. Particles with a dry mobility diameter of 100 nm were selected and exposed to controlled RH conditions ranging from 10% to 93%. Their humidified size distributions were then measured to determine hygroscopic growth. The growth factor at 90% RH, g(90%), was used to compare samples collected at different sites and during different seasons. The H-TDMA system was routinely checked using ammonium sulfate particles.

2.3.2 Hygroscopicity measurements of separated water-soluble inorganic and organic fractions

To quantify the contributions of inorganic and organic components to aerosol hygroscopicity, the bulk water-soluble extracts were separated into water-soluble inorganic matter (WSIM) and water-soluble organic matter (WSOM) using Oasis HLB solid-phase extraction (SPE) cartridges (Waters, USA). Filtered aqueous extracts were loaded onto the SPE cartridges under vacuum. The initial aqueous eluate, followed by a 3 mL ultrapure water rinse, was collected as the WSIM fraction. Organic compounds retained on the cartridge were then eluted twice with 3 mL methanol. The combined methanol eluates were evaporated to near dryness under a gentle nitrogen stream and reconstituted in ultrapure water to obtain the WSOM fraction for subsequent hygroscopicity measurements.

The separation efficiency was evaluated using three randomly selected $PM_{2.5}$ samples. Sulfate and nitrate concentrations were determined before and after SPE separation. Recoveries of sulfate and nitrate in the inorganic fraction exceeded 87% for all three samples, whereas both ions were below the detection limits in the organic fraction, demonstrating effective separation of the major inorganic components (Table S1). The WSIM and WSOM solutions were subsequently atomized and analyzed using the same H-TDMA procedure as described for the bulk water-soluble extracts.

2.4 Hygroscopicity calculation

2.4.1 Hygroscopic growth factor

The hygroscopic growth factor, g(RH), was calculated from the ratio of the humidified to dry particle diameter (Eq. 1). The humidified diameter was determined from lognormal fits to the measured particle size distributions (Boreddy et al., 2016; Swietlicki et al., 2008):

https://doi.org/10.5194/egusphere-2026-6766
Preprint. Discussion started: 19 November 2026
© Author(s) 2026. CC BY 4.0 License.

$$g(\mathrm{RH}) = \frac{D_p(\mathrm{RH})}{D_{dry}} \quad (1)$$

2.4.2 Hygroscopicity parameter (κ) and ZSR calculation

The hygroscopicity parameter (κ) was calculated from the measured growth factors using the κ-Köhler framework (Petters and Kreidenweis, 2007) following Eqs. (2)–(4) (Petters and Kreidenweis, 2007; Swietlicki et al., 2008):

$$\kappa = \frac{\left[g(\mathrm{RH})^3 - 1\right](1 - a_w)}{a_w} \quad (2)$$

$$a_w = \frac{\mathrm{RH}}{100}\left[\exp\left(\frac{A}{g(\mathrm{RH})D_0}\right)\right]^{-1} \quad (3)$$

with

$$A = \frac{4\sigma_{s/a}M_w}{\rho_w RT} \quad (4)$$

where a_w is the water activity, $\sigma_{s/a}$ is the surface tension at the solution–air interface, M_w and ρ_w are the molar mass and density of water, respectively; R is the universal gas constant; T is the absolute temperature; and D_0 is the droplet diameter.

The hygroscopic growth of WSIM was also estimated from its ionic composition using the Zdanovskii–Stokes–Robinson (ZSR) mixing rule (Eq. 5), which assumes additive water uptake by individual components (Bouzidi et al., 2020; Luo et al., 2020). Here, $g_i(\mathrm{RH})$ represents the growth factor of component i, and ε_i is its volume fraction in the mixture. Calculations were performed with and without K^+-, Ca^{2+}-, and Mg^{2+}-containing species to examine their influence on the predicted WSIM hygroscopicity.

$$g(\mathrm{RH})_{WSM} = \left\{\sum_i \left[\varepsilon_i g_i^3(\mathrm{RH})\right]\right\}^{1/3} \quad (5)$$

2.5 Air mass backward trajectory analysis and potential source contribution function

Backward trajectories were calculated using MeteoInfoMap to investigate air mass transport pathways and potential source regions of $PM_{2.5}$ at the summit and foothill sites. For each sampling period, 48 h backward trajectories were calculated with a new trajectory initiated every 6 h. The trajectories were initialized at the corresponding elevations of the sampling sites (2060 m a.s.l. for

https://doi.org/10.5194/egusphere-2026-6766
Preprint. Discussion started: 19 November 2026
© Author(s) 2026. CC BY 4.0 License.

the summit site and 385 m a.s.l. for the foothill site). Cluster analysis was applied to classify trajectories and identify dominant air mass transport patterns.

The PSCF analysis was performed to identify potential source regions of $PM_{2.5}$ (Yang et al., 2025). The Class I daily $PM_{2.5}$ standard in China was used as the threshold value for defining polluted air masses. Due to the relatively low $PM_{2.5}$ concentrations at the summit site during summer, PSCF analysis was only conducted for summer foothill samples and winter samples from both sites.

3. Results and discussion

3.1 Seasonal and vertical variations in $PM_{2.5}$ and water-soluble matter

Table 1 summarizes the average concentrations of $PM_{2.5}$ and the major water-soluble species at Mt. Hua, with their temporal variations shown in Figure S2 and Figure 1, respectively. Clear seasonal, diurnal, and vertical variations were observed in $PM_{2.5}$ and its water-soluble species. $PM_{2.5}$ and all measured water-soluble species were substantially higher in winter than in summer at both the summit and foothill sites. The wintertime enhancement was particularly pronounced at the foothill, where $PM_{2.5}$ increased from 31.49 ± 14.59 to 138.29 ± 74.71 μg m^{-3}, compared with an increase from 10.70 ± 6.15 to 31.89 ± 26.41 μg m^{-3} at the summit. Such enhanced wintertime aerosol loading is generally observed in the Guanzhong plain and can be attributed to increased combustion and heating emissions, stronger accumulation under stagnant conditions, and enhanced partitioning of semi-volatile species into the particle phase at lower temperatures (Wang et al., 2022; Niu et al., 2016). Among the WSM, NO_3^- showed one of the largest seasonal increases, rising from 2.77 ± 2.55 to 15.95 ± 12.97 μg m^{-3} at the foothill and from 0.38 ± 0.53 to 4.37 ± 4.56 μg m^{-3} at the summit. The pronounced increase in particulate nitrate is consistent with enhanced wintertime precursor emissions and more favorable partitioning of nitrate to the particle phase at low temperatures (Wen et al., 2025; Morino et al., 2006).

https://doi.org/10.5194/egusphere-2026-6766
Preprint. Discussion started: 19 November 2026
© Author(s) 2026. CC BY 4.0 License.

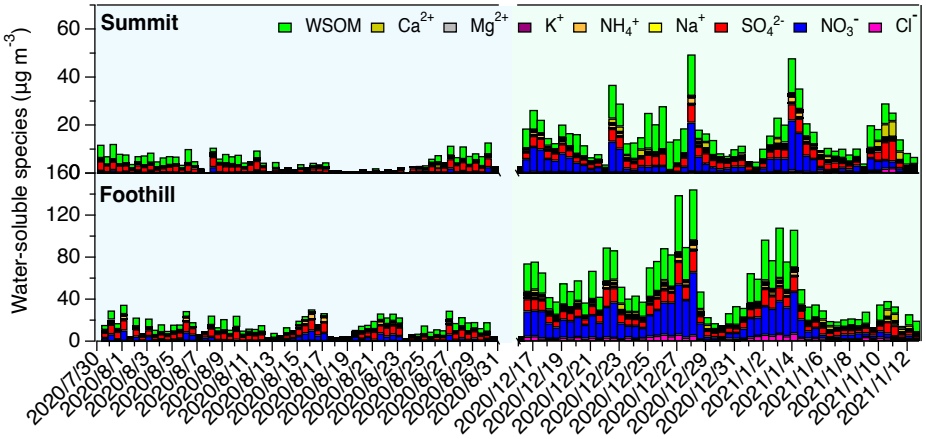


Figure 1. Temporal variations in the concentrations of major water-soluble species at the summit and foothill sites of Mt. Hua during summer and winter.

A daytime–nighttime contrast was also evident, with $PM_{2.5}$ and most water-soluble species generally higher during daytime than nighttime, particularly at the foothill. This pattern likely reflects stronger daytime emissions and atmospheric mixing associated with human activities and enhanced surface–atmosphere exchange, whereas weaker emissions and a more stable nocturnal boundary layer may suppress aerosol production and transport (Zografou et al., 2024).

In terms of the vertical variation, $PM_{2.5}$ and most water-soluble species were consistently more abundant at the foothill than at the summit, and this vertical difference was more apparent in winter. Similar vertical gradients have been reported at Mt. Hua and other mountain environments, reflecting the stronger influence of surface emissions at the foothill and incomplete vertical mixing between the polluted boundary layer and the mountain atmosphere (Feng et al., 2023; Yi et al., 2021; Kwon et al., 2025). The enhanced wintertime gradient likely reflects stronger accumulation of locally and regionally emitted aerosols near the surface under stagnant atmospheric conditions, which limits their vertical dilution and transport to the summit. The vertical difference was also generally larger during daytime than nighttime. This may partly reflect stronger daytime surface emissions at the foothill, which could enhance near-surface aerosol concentrations, while the effects of these emissions at the summit depend on subsequent vertical transport and atmospheric dilution, potentially contributing to a larger daytime concentration gradient between the two elevations (Vitali et al., 2024; Zhang et al., 2012).

https://doi.org/10.5194/egusphere-2026-6766
Preprint. Discussion started: 19 November 2026
© Author(s) 2026. CC BY 4.0 License.

Beyond aerosol loading, the relative contributions of individual water-soluble species also differed between the summit and foothill sites (Figure 2). In summer, NO_3^- and NH_4^+ accounted for larger fractions at the foothill than at the summit (17.9% vs. 7.3% for NO_3^- and 8.9% vs. 1.4% for NH_4^+), whereas WSOM showed the opposite vertical pattern (44.1% at the summit vs. 33.6% at the foothill). Na^+ also contributed a relatively larger fraction at the summit. The higher fractions of NO_3^- and NH_4^+ at the foothill likely reflect the stronger influence of surface-level anthropogenic emissions and secondary inorganic aerosol formation, while the enhanced WSOM fraction at the summit may reflect differences in the sources and atmospheric processing of organic aerosol between the two elevations. In winter, Cl^- showed a higher fraction at the foothill, whereas Ca^{2+} contributed a larger fraction at the summit (6.5% vs. 4.7%). The enhanced Ca^{2+} fraction at the summit may reflect a greater contribution of mineral-containing aerosol at the higher elevation. Other major components, including WSOM, NO_3^-, and SO_4^{2-}, showed relatively small differences in their fractional contributions between the two elevations.

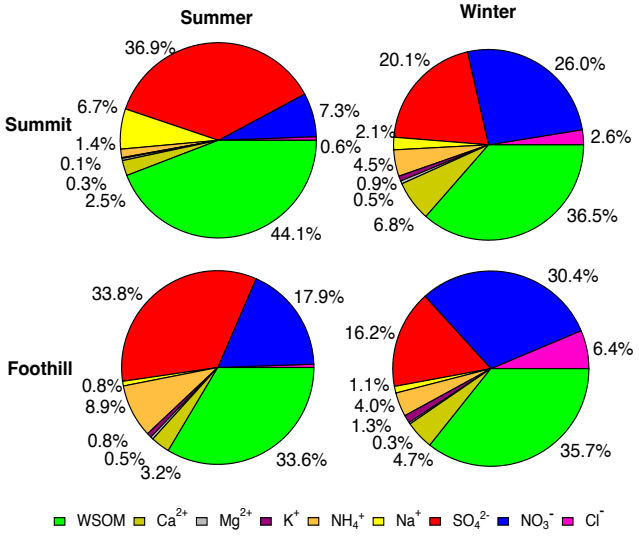


Figure 2. Relative contributions of individual water-soluble species to total water-soluble matter at the summit and foothill sites of Mt. Hua during summer and winter.

Short-term meteorological conditions also affected the observed aerosol distributions. Distinct rainfall and high-RH episodes occurred in summer, whereas several cooling episodes accompanied by stronger winds were observed in winter (Figure S3). During summer rainfall and fog periods, $PM_{2.5}$ and WSM concentrations decreased at both the summit and foothill (Figure 1), consistent

https://doi.org/10.5194/egusphere-2026-6766
Preprint. Discussion started: 19 November 2026
© Author(s) 2026. CC BY 4.0 License.

with enhanced wet removal under humid conditions (Chen et al., 2025; Jones et al., 2022). Changes in the relative contributions of individual water-soluble species (Table S2) further indicate that precipitation affected aerosol composition in addition to total aerosol loading. In winter, cooling episodes were accompanied by stronger winds and reduced $PM_{2.5}$ and WSM concentrations at both summit and foothill sites, consistent with enhanced atmospheric dispersion, along with changes in WSM composition (Table S2).

Overall, the observations show substantial seasonal and vertical differences in both aerosol loading and water-soluble composition, with the strongest concentration contrast occurring between the summit and foothill during winter. The differences in chemical composition further suggest that the two elevations were affected by different mixtures of locally influenced and transported aerosols.

3.2 Air mass transport and potential source regions

To further identify the origins and potential source regions of transported aerosols, backward trajectory and PSCF analyses were conducted. Figure 3 shows the clustered backward trajectories for the summit and foothill sites during summer and winter, with the corresponding variations in air-mass height along the 48-h trajectories provided in Figure S4. In summer, the two sites were influenced by distinctly different transport pathways. At the summit, air masses originated mainly from the southwest (Cluster 3, 49.22%) and southeast (Cluster 1, 32.81%), with a smaller contribution from the northwest (17.97%). By comparison, the foothill was dominated by relatively short-range transport from the southeast (57.03%) and northwest (30.47%). The shorter and lower-altitude trajectories at the foothill imply a stronger influence of surface emissions from surrounding populated areas, including NO_x and NH_3 precursors, which may partly explain the larger fractions of NO_3^- and NH_4^+ observed there (Xue et al., 2023). At the summit, the greater contribution of southwesterly air masses with longer transport pathways may have allowed more extensive atmospheric processing of organic aerosol, thereby increasing its water solubility and contributing to the relatively larger WSOM fraction (Li et al., 2021; Kirillova et al., 2013).

https://doi.org/10.5194/egusphere-2026-6766
Preprint. Discussion started: 19 November 2026
© Author(s) 2026. CC BY 4.0 License.

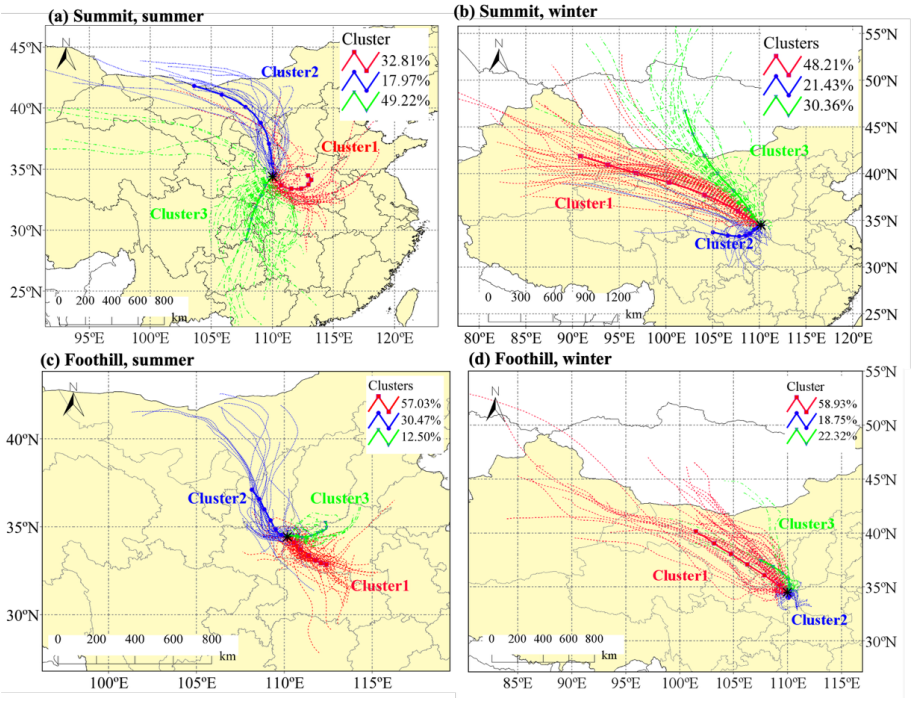


Figure 3. Clustered 48-h backward trajectories of air masses arriving at the Mt. Hua summit (a, b) and foothill (c, d) sites.

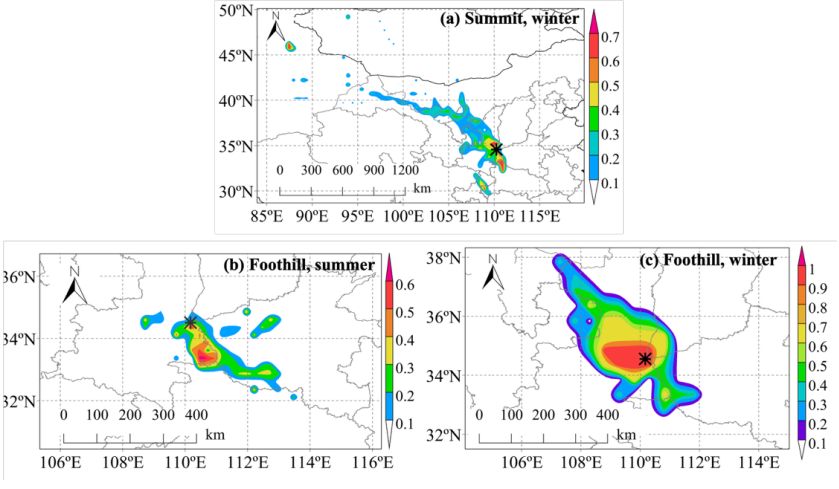
Table S3 further summarizes the distribution of trajectory clusters under different meteorological conditions. During rainy and foggy periods, the southwestern and southeastern clusters contributed 20.31% and 10.16% of the total trajectories at the summit, respectively, compared with only 0.78% from the northwest. At the foothill, the corresponding trajectories were more evenly distributed among the southeastern (15.63%), northwestern (14.06%), and eastern (10.94%) clusters. Thus, in addition to wet scavenging, differences in air mass origin may have contributed to the changes in aerosol composition observed during rainy and foggy periods (Table S2).

The difference in air mass origins between the two elevations became much smaller in winter, when northwesterly transport dominated at both sites. The two northwesterly clusters accounted for 48.21% and 30.36% of the trajectories at the summit and 58.93% and 22.32% at the foothill, respectively. The similar transport patterns are consistent with the relatively small summit–foothill differences in the fractional contributions of major components such as WSOM, NO_3^-, and SO_4^{2-} in winter. Northwesterly transport was also closely associated with the cooling episodes (Table S3).

https://doi.org/10.5194/egusphere-2026-6766
Preprint. Discussion started: 19 November 2026
© Author(s) 2026. CC BY 4.0 License.

294 At the summit, the two northwesterly clusters contributed 12.50% and 22.32% of the total
295 trajectories during cooling periods, while the southwestern cluster contributed only 0.89%. At the
296 foothill, the dominant northwesterly cluster contributed 29.46%, whereas no cooling-period
297 trajectories were associated with the southwestern cluster. As these northwesterly air masses
298 passed over northwestern China and the Loess Plateau before reaching Mt. Hua, they may have
299 transported more mineral-containing aerosol (Shen et al., 2025; Zhang et al., 1993), consistent with
300 the higher Ca^{2+} fractions during cooling periods (Table S2).

301 The PSCF results provide further evidence for the different source influences at the two
302 elevations (Figure 4). In summer, the major potential source regions for $PM_{2.5}$ at the foothill were
303 located southeast of Mt. Hua, particularly over southeastern Shaanxi and southwestern Henan,
304 supporting the stronger influence of surrounding source regions inferred from the trajectories. In
305 winter, elevated PSCF values at the summit extended predominantly toward the northwest,
306 consistent with regional transport, whereas the highest PSCF values at the foothill were
307 concentrated around the sampling region. This may explain why the wintertime foothill–summit
308 concentration difference remained large despite their broadly similar air mass origins, as the
309 foothill was additionally influenced by local and nearby regional sources.



310

311 **Figure 4.** PSCF distributions of $PM_{2.5}$ at Mt. Hua for the summit site in winter (a), the foothill site
312 in summer (b), and the foothill site in winter (c).

313

314 3.3 Seasonal and vertical variations in WSM hygroscopicity

https://doi.org/10.5194/egusphere-2026-6766
Preprint. Discussion started: 19 November 2026
© Author(s) 2026. CC BY 4.0 License.

Figure 5 shows the temporal variations in $g(90\%)_{WSM}$ and κ_{WSM} at the summit and foothill during summer and winter. At the summit, $g(90\%)_{WSM}$ averaged 1.49 ± 0.06 in summer and decreased to 1.34 ± 0.07 in winter, with corresponding κ_{WSM} values of 0.30 ± 0.05 and 0.18 ± 0.05, respectively. At the foothill, $g(90\%)_{WSM}$ similarly decreased from 1.41 ± 0.13 in summer to 1.30 ± 0.05 in winter, while κ_{WSM} decreased from 0.24 ± 0.10 to 0.16 ± 0.03. The wintertime κ_{WSM} at the summit was comparable to an in situ HTDMA measurement at the same Mt. Hua summit, where κ increased from 0.20 ± 0.06 to 0.30 ± 0.05 for 30–200 nm ambient particles, with a value of 0.25 ± 0.05 at 100 nm (Shi et al., 2026). Although the two measurements are not directly equivalent because our offline approach characterizes the extracted water-soluble fraction, their comparable values support the atmospheric relevance of the WSM hygroscopicity determined here. More broadly, our κ_{WSM} values fall within the range of approximately 0.15–0.35 reported for aerosols at high-altitude sites worldwide (Shi et al., 2026). The substantial variability in aerosol hygroscopicity among mountain sites has been related to differences in aerosol sources and atmospheric processing, with aged and secondary-inorganic-rich aerosols generally being more hygroscopic than aerosols strongly influenced by less-aged boundary-layer emissions or mineral dust.

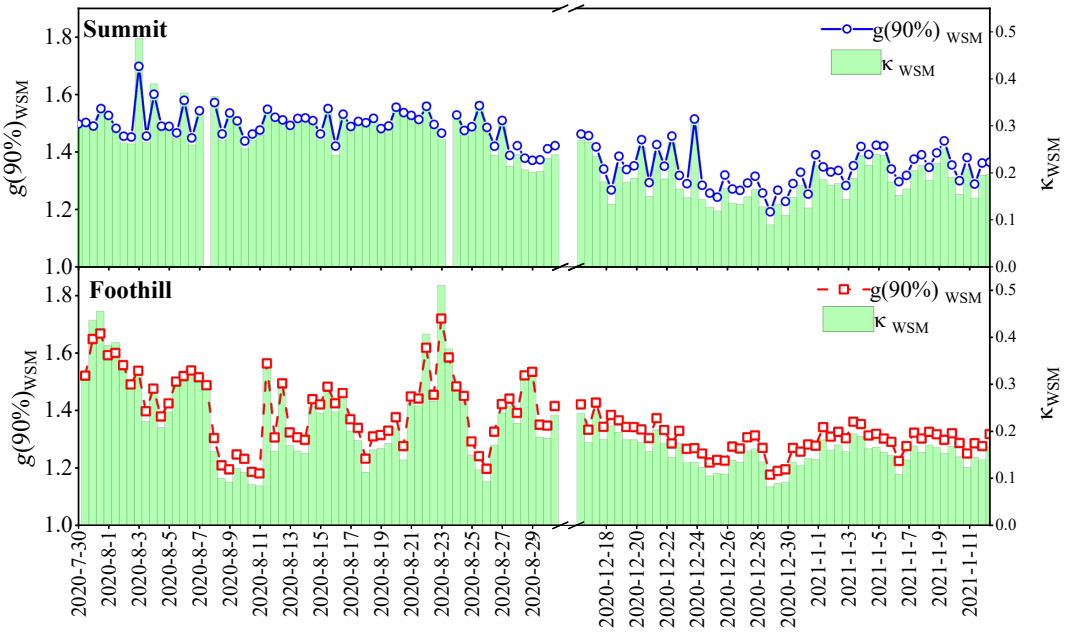


Figure 5. Temporal variations in $g(90\%)_{WSM}$ and κ_{WSM} at the summit and foothill.

https://doi.org/10.5194/egusphere-2026-6766
Preprint. Discussion started: 19 November 2026
© Author(s) 2026. CC BY 4.0 License.

A clear seasonal difference in WSM hygroscopicity was observed at both elevations, with significantly higher $g(90\%)_{WSM}$ and κ_{WSM} in summer than in winter ($p < 0.0001$). The contrast can be linked to the substantial seasonal shift in WSM composition (Figure 2). Summer aerosols contained a greater relative contribution of SO_4^{2-}, whereas winter aerosols showed enhanced contributions from biomass burning (BB)- related and mineral-related species, as indicated by higher fractions of K^+ (accompanied by elevated Cl^-) and Ca^{2+}, respectively (Andreae, 2019; Shen et al., 2007). Sulfate salts such as ammonium sulfate are highly hygroscopic and contribute efficiently to aerosol water uptake, whereas BB-derived organic matter and mineral-dust-influenced aerosols generally exhibit lower hygroscopicity (Swietlicki et al., 2008; Lei et al., 2014; Koehler et al., 2009). These compositional differences likely contributed to the higher WSM hygroscopicity observed in summer. In addition, a significant vertical contrast in WSM hygroscopicity, with significantly higher values at the summit than at the foothill, was observed in both seasons ($p < 0.0001$), although this vertical difference was less pronounced in winter. This pattern can be linked to the contrasting air-mass transport and chemical characteristics. During summer, the summit was more strongly influenced by regional and long-range transported air masses (Figure 3) and showed relatively higher contributions from both SO_4^{2-} and WSOM (Figure 2), suggesting a greater influence of atmospherically processed secondary aerosol. In winter, northwesterly air masses dominated at both elevations, reducing the compositional contrast between the summit and foothill, which may partly explain the smaller vertical difference in WSM hygroscopicity. In contrast to these significant seasonal and vertical variations, no significant daytime–nighttime difference in $g(90\%)_{WSM}$ was found at either elevation in either season, suggesting that WSM hygroscopicity was influenced more strongly by seasonal changes in aerosol sources, composition, and regional transport than by diurnal variability.

To further evaluate the compositional controls, Spearman correlations were examined between $g(90\%)_{WSM}$ and the relative contributions of major WSM components (Figure 6). When all samples were considered together, $g(90\%)_{WSM}$ was positively correlated with the SO_4^{2-} fraction at both the summit ($r = 0.46$, $p < 0.001$) and foothill ($r = 0.42$, $p < 0.001$), but negatively correlated with K^+ ($r = -0.65$, $p < 0.001$ and $r = -0.51$, $p < 0.001$, respectively; scatter plots shown in Figure S5). These opposite relationships further point to the contrasting influences of sulfate-rich secondary aerosol and BB-influenced WSM on aerosol hygroscopicity. However, most of these correlations weakened or disappeared when the data were separated by season, indicating that the strong

https://doi.org/10.5194/egusphere-2026-6766
Preprint. Discussion started: 19 November 2026
© Author(s) 2026. CC BY 4.0 License.

campaign-wide relationships were driven partly by seasonal covariation between aerosol composition and hygroscopicity (Figure 6). The remaining within-season relationships differed between elevations. At the summit, no individual component showed a significant relationship with $g(90\%)_{WSM}$ in summer, while only relatively weak correlations were observed with NO_3^- and Mg^{2+} in winter. In contrast, clearer relationships were found at the foothill, including negative correlations with WSOM and K^+ in summer and positive correlations with NO_3^- in both seasons.

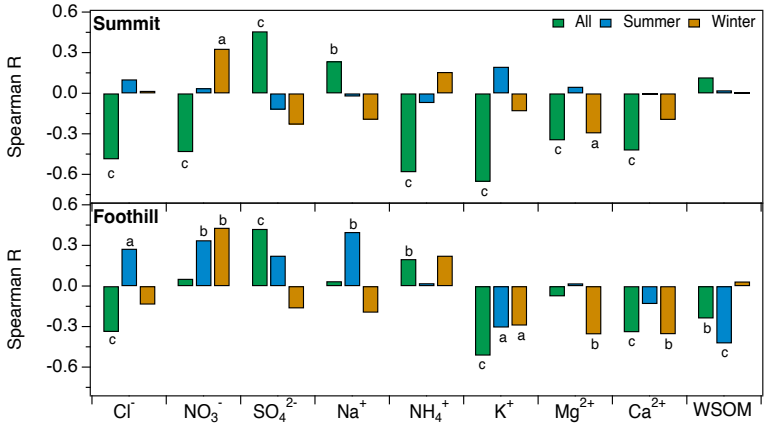


Figure 6. Spearman correlation coefficients between $g(90\%)_{WSM}$ and the relative contributions of major water-soluble components at the summit and foothill for all samples and separately for summer and winter. a, b, and c indicate statistical significance at $p < 0.05$, $p < 0.01$, and $p < 0.001$, respectively.

Overall, the seasonal and vertical variations in WSM hygroscopicity were closely associated with changes in aerosol sources, transport, and chemical composition. However, the weak and inconsistent correlations with individual components within each season indicate that the observed hygroscopicity cannot be explained by variations in major water-soluble species alone. Instead, the balance between inorganic and organic water-soluble components, together with differences in their hygroscopic properties, may collectively regulate WSM hygroscopicity.

3.4 Hygroscopicity of water-soluble inorganic and organic fractions

To investigate the hygroscopicity of WSIM and WSOM, selected samples were separated into predominantly organic and inorganic fractions using solid-phase extraction. Figure 7 shows the measured hygroscopicity of the two separated fractions. The WSIM fraction was consistently more

https://doi.org/10.5194/egusphere-2026-6766
Preprint. Discussion started: 19 November 2026
© Author(s) 2026. CC BY 4.0 License.

hygroscopic and showed greater sample-to-sample variability than the WSOM fraction at both elevations. At the summit, both fractions showed higher average g(90%) in summer than in winter, following the seasonal pattern observed for bulk WSM. At the foothill, however, the seasonal pattern differed from that of bulk WSM. The WSIM fraction was slightly more hygroscopic in winter than in summer, while the WSOM fraction showed little seasonal difference, despite the significantly higher bulk WSM hygroscopicity in summer. Thus, the seasonal variation in bulk WSM hygroscopicity cannot be explained simply by corresponding changes in the hygroscopicity of either separated fraction, but likely reflects the combined effects of their hygroscopic properties and relative contributions to WSM.

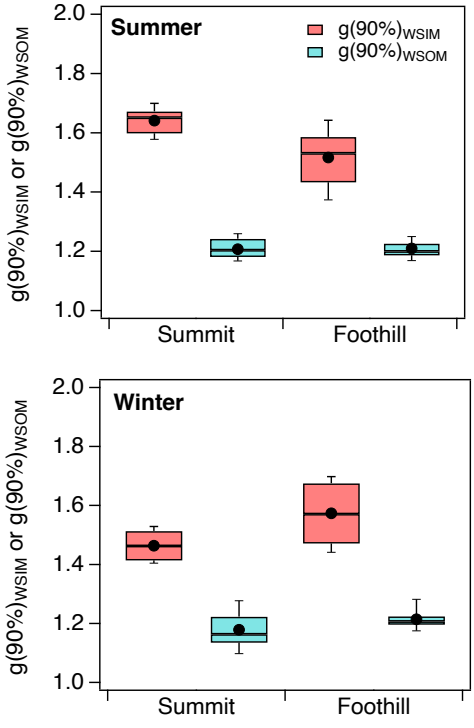


Figure 7. $g(90\%)_{WSIM}$ and $g(90\%)_{WSOM}$ of the separated water-soluble inorganic and organic fractions at the summit and foothill during summer and winter. The boxes represent the 25th percentile, median (solid line), mean (solid dot), and 75th percentile. The whiskers represent the 10th percentile and 90th percentile.

https://doi.org/10.5194/egusphere-2026-6766
Preprint. Discussion started: 19 November 2026
© Author(s) 2026. CC BY 4.0 License.

To further examine the influence of inorganic composition, $g(90\%)_{WSIM}$ was calculated from the measured ionic composition using the ZSR mixing rule and compared with the HTDMA measurements. The ZSR approach has been widely used to predict aerosol hygroscopic growth from the volume fractions and hygroscopic properties of individual components (Healy et al., 2014; Bouzidi et al., 2020). Figure 8 shows the differences between calculated and measured $g(90\%)_{WSIM}$ for calculations performed with and without K^+-, Ca^{2+}-, and Mg^{2+}-containing species. When K^+-, Ca^{2+}-, and Mg^{2+}-containing species were excluded, the calculations generally overestimated the measured $g(90\%)_{WSIM}$ at both elevations and in both seasons. Including these species substantially reduced the model–measurement differences, particularly in winter. The mean differences between calculated and measured $g(90\%)_{WSIM}$ decreased to 0.21 ± 0.12 and 0.11 ± 0.21 at the summit and foothill in summer, respectively, and to 0.10 ± 0.16 and 0.02 ± 0.18 in winter. The close agreement in the average values for the winter foothill samples was particularly evident, whereas larger discrepancies remained for the summer samples. These results show that inclusion of K^+-, Ca^{2+}-, and Mg^{2+}-containing species improves the representation of the overall magnitude of WSIM hygroscopicity. Nevertheless, the remaining discrepancies indicate that the measured water uptake cannot be fully represented by the reconstructed inorganic composition, likely reflecting uncertainties in the assumed salt forms and mixing state as well as the simplified additivity in the ZSR calculation (Swietlicki et al., 2008; Zhou et al., 2024; Razafindrambinina et al., 2022).

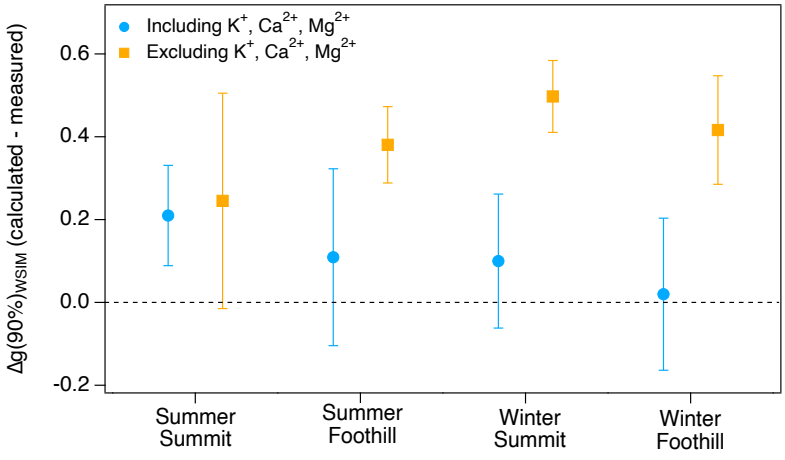


Figure 8. Differences between ZSR-calculated and measured $g(90\%)_{WSIM}$ at the summit and foothill during summer and winter. ZSR calculations were performed with and without K^+-, Ca^{2+}-,

https://doi.org/10.5194/egusphere-2026-6766
Preprint. Discussion started: 19 November 2026
© Author(s) 2026. CC BY 4.0 License.

and Mg^{2+}-containing species. Symbols and error bars represent the mean and standard deviation, respectively. Positive values indicate overestimation of the measured hygroscopic growth.

Spearman correlation analysis was further used to examine the relationships between measured $g(90\%)_{WSIM}$ and the relative contributions of individual ions (Figure S6). At the summit, significant correlations with several ions were observed when all samples were considered together, including a positive correlation with SO_4^{2-} ($r = 0.52$, $p < 0.001$) and a negative correlation with K^+ ($r = -0.72$, $p < 0.001$). However, most of these relationships disappeared when the data were analyzed separately by season. No significant correlations were observed in summer, while Ca^{2+} was negatively correlated with $g(90\%)_{WSIM}$ in winter ($r = -0.58$, $p < 0.05$). At the foothill, no consistent relationships between $g(90\%)_{WSIM}$ and individual ions were observed. Consistent with the model results, these suggest that variations in WSIM hygroscopicity are related to changes in multiple inorganic components rather than to any single major ion.

Overall, the separation experiments demonstrate the contrasting hygroscopic properties of the water-soluble inorganic and organic fractions. The inorganic fraction showed substantially greater water uptake and greater variability than the organic fraction, while its hygroscopicity could be better reproduced when a broader range of inorganic species was included in the ZSR calculation.

4. Conclusions

This study investigated the seasonal and vertical variations in the composition and hygroscopicity of $PM_{2.5}$ water-soluble matter at the summit and foothill of Mt. Hua. WSM hygroscopicity was significantly higher in summer than in winter and at the summit than at the foothill, despite substantially higher aerosol loadings in winter and at the foothill. These differences were accompanied by changes in chemical composition and air-mass transport, with greater contributions of sulfate-rich and more regionally transported aerosol associated with higher hygroscopicity, whereas biomass-burning- and mineral-influenced aerosol became more important in winter. However, the relationships between hygroscopicity and individual components generally weakened when the samples were separated by season, indicating that the apparent compositional dependence partly reflected seasonal changes in aerosol sources and transport.

Separation of WSM further showed that the inorganic fraction was substantially more hygroscopic than the organic fraction, but the seasonal variation in bulk WSM hygroscopicity did not simply follow that of either fraction. Including K^+-, Ca^{2+}-, and Mg^{2+}-containing species

https://doi.org/10.5194/egusphere-2026-6766
Preprint. Discussion started: 19 November 2026
© Author(s) 2026. CC BY 4.0 License.

improved the ZSR prediction of inorganic hygroscopicity, while the remaining discrepancies suggest that inorganic speciation and interactions among components also affect water uptake. Overall, these results suggest that aerosol hygroscopicity in mountain environments reflects the combined effects of source and transport history, organic–inorganic partitioning, and detailed chemical composition, rather than variations in aerosol loading or individual chemical components alone. Aerosol sources, atmospheric processing, and multicomponent chemical composition should therefore be considered together when interpreting variations in aerosol hygroscopicity.

Data availability

The data are available at https://doi.org/10.5281/zenodo.23855218 (Wang and Li, 2026).

Author contributions

XW and JL designed the research. XW, YC, JW, BL, YL, YZ, YC, MS, WD, LL, and XG carried out the experiments. JL, FL, and YW supervised the study. XW and JL prepared the original manuscript with input from all the co-authors.

Competing interests

The authors declare that they have no conflicts of interest.

Disclaimer

Publisher's note: Copernicus Publications remains neutral with regard to jurisdictional claims made in the text, published maps, institutional affiliations, or any other geographical representation in this paper. While Copernicus Publications makes every effort to include appropriate place names, the final responsibility lies with the authors.

Financial support

This work is supported by the Natural Science Basic Research Program of Shaanxi Province (2025JC-YBQN-341) and the National Natural Science Foundation of China (42577120).

References

https://doi.org/10.5194/egusphere-2026-6766
Preprint. Discussion started: 19 November 2026
© Author(s) 2026. CC BY 4.0 License.

Andreae, M. O.: Emission of trace gases and aerosols from biomass burning–an updated assessment, Atmospheric Chemistry and Physics, 19, 8523-8546, 10.5194/acp-19-8523-2019, 2019.
Boreddy, S., Kawamura, K., Bikkina, S., and Sarin, M.: Hygroscopic growth of particles nebulized from water-soluble extracts of PM2.5 aerosols over the Bay of Bengal: Influence of heterogeneity in air masses and formation pathways, Science of the Total Environment, 544, 661-669, 10.1016/j.scitotenv.2015.11.164, 2016.
Boreddy, S. K. R. and Kawamura, K.: Hygroscopic growth of water-soluble matter extracted from remote marine aerosols over the western North Pacific: Influence of pollutants transported from East Asia, Science of The Total Environment, 557-558, 285-295, 10.1016/j.scitotenv.2016.03.096, 2016.
Bouzidi, H., Zuend, A., Ondráček, J., Schwarz, J., and Ždímal, V.: Hygroscopic behavior of inorganic–organic aerosol systems including ammonium sulfate, dicarboxylic acids, and oligomer, Atmospheric Environment, 229, 117481, 10.1016/j.atmosenv.2020.117481, 2020.
Chen, S., Liu, M., Zou, S., Xu, H., and Zhang, F.: Unveiling the dual role of rainfall in governing ambient aerosol particles: From washout-dominated scavenging to production dynamics, Atmospheric Environment, 121513, 10.1016/j.atmosenv.2025.121513, 2025.
Chen, Y., Wang, X., Peng, H., Li, J., Wang, Y., Wang, G., Li, J., Wu, C., and Liu, L.: Hygroscopicity of Water-Soluble PM2.5 in Rural Northwest China: Contrasting Contributors Between Summer and Winter, Journal of Geophysical Research: Atmospheres, 126, e2021JD034977, 10.1029/2021JD034977, 2021.
Chen, Y., Wang, X., Dai, W., Wang, Q., Guo, X., Liu, Y., Qi, W., Shen, M., Zhang, Y., Li, L., Cao, Y., Wang, Y., and Li, J.: Particle Number Size Distribution of Wintertime Alpine Aerosols and Their Activation as Cloud Condensation Nuclei in the Guanzhong Plain, Northwest China, Journal of Geophysical Research: Atmospheres, 128, e2022JD037877, 10.1029/2022JD037877, 2023.
Collaud Coen, M., Andrews, E., Aliaga, D., Andrade, M., Angelov, H., Bukowiecki, N., Ealo, M., Fialho, P., Flentje, H., Hallar, A. G., Hooda, R., Kalapov, I., Krejci, R., Lin, N. H., Marinoni, A., Ming, J., Nguyen, N. A., Pandolfi, M., Pont, V., Ries, L., Rodríguez, S., Schauer, G., Sellegri, K., Sharma, S., Sun, J., Tunved, P., Velasquez, P., and Ruffieux, D.: Identification of topographic features influencing aerosol observations at high altitude stations, Atmos. Chem. Phys., 18, 12289-12313, 10.5194/acp-18-12289-2018, 2018.
Duplissy, J., DeCarlo, P. F., Dommen, J., Alfarra, M. R., Metzger, A., Barmpadimos, I., Prevot, A. S. H., Weingartner, E., Tritscher, T., and Gysel, M.: Relating hygroscopicity and composition of organic aerosol particulate matter, Atmospheric Chemistry and Physics, 11, 1155-1165, 10.5194/acp-11-1155-2011, 2011.
Feng, Q., Liu, H., Dai, W., Cao, Y., Shen, M., Liu, Y., Qi, W., Chen, Y., Guo, X., and Zhang, Y.: Comparison of chemical composition and acidity of size-resolved inorganic aerosols at the top and foot of Mt. Hua, Northwest China: The role of the gas-particle distribution of ammonia, Science of the Total Environment, 905, 166985, 10.1016/j.scitotenv.2023.166985, 2023.
Gysel, M., Weingartner, E., Nyeki, S., Paulsen, D., Baltensperger, U., Galambos, I., and Kiss, G.: Hygroscopic properties of water-soluble matter and humic-like organics in atmospheric fine aerosol, Atmos. Chem. Phys., 4, 35-50, 10.5194/acp-4-35-2004, 2004.
Healy, R. M., Evans, G. J., Murphy, M., Jurányi, Z., Tritscher, T., Laborde, M., Weingartner, E., Gysel, M., Poulain, L., and Kamilli, K. A.: Predicting hygroscopic growth using single particle chemical composition estimates, Journal of Geophysical Research: Atmospheres, 119, 9567-9577, 10.1002/2014JD021888, 2014.
Holmgren, H., Sellegri, K., Hervo, M., Rose, C., Freney, E., Villani, P., and Laj, P.: Hygroscopic properties and mixing state of aerosol measured at the high-altitude site Puy de Dôme (1465 m a.s.l.), France, Atmos. Chem. Phys., 14, 9537-9554, 10.5194/acp-14-9537-2014, 2014.
Jones, A. C., Hill, A., Hemmings, J., Lemaitre, P., Quérel, A., Ryder, C., and Woodward, S.: Below-cloud scavenging of aerosol by rain: A review of numerical modelling approaches and sensitivity simulations with mineral dust, Atmospheric Chemistry and Physics, 22, 11381-11407, 10.5194/acp-22-11381-2022, 2022.
Kirillova, E. N., Andersson, A., Sheesley, R. J., Kruså, M., Praveen, P., Budhavant, K., Safai, P., Rao, P., and Gustafsson, Ö.: 13C-and 14C-based study of sources and atmospheric processing of water-soluble organic carbon (WSOC) in South Asian aerosols, Journal of Geophysical Research: Atmospheres, 118, 614-626, 10.1002/jgrd.50130, 2013.

https://doi.org/10.5194/egusphere-2026-6766
Preprint. Discussion started: 19 November 2026
© Author(s) 2026. CC BY 4.0 License.

Koehler, K., Kreidenweis, S., DeMott, P., Petters, M., Prenni, A., and Carrico, C.: Hygroscopicity and cloud droplet activation of mineral dust aerosol, Geophysical Research Letters, 36, 10.1029/2009GL037348, 2009.
Kwon, S., Hu, Q., Seo, J., Park, S., Moon, J., Kim, J., Park, S., Park, Y., and Kim, H.: Characterization of particulate matter at Mt. Gwanak (at 632 m) and vertical mixing impacts on haze in Seoul during winter, Science of the Total Environment, 958, 178106, 10.1016/j.scitotenv.2024.178106, 2025.
Lei, T., Zuend, A., Wang, W., Zhang, Y., and Ge, M.: Hygroscopicity of organic compounds from biomass burning and their influence on the water uptake of mixed organic ammonium sulfate aerosols, Atmospheric Chemistry and Physics, 14, 11165-11183, 10.5194/acp-14-11165-2014, 2014.
Li, H., Zhang, Q., Jiang, W., Collier, S., Sun, Y., Zhang, Q., and He, K.: Characteristics and sources of water-soluble organic aerosol in a heavily polluted environment in Northern China, Science of the Total Environment, 758, 143970, 10.1016/j.scitotenv.2020.143970, 2021.
Li, J., Wang, G., Zhou, B., Cheng, C., Cao, J., Shen, Z., and An, Z.: Chemical composition and size distribution of wintertime aerosols in the atmosphere of Mt. Hua in central China, Atmospheric Environment, 45, 1251-1258, 10.1016/j.atmosenv.2010.12.009, 2011.
Li, J., Zhang, Q., Wang, G., Li, J., Wu, C., Liu, L., Wang, J., Jiang, W., Li, L., and Ho, K. F.: Optical properties and molecular compositions of water-soluble and water-insoluble brown carbon (BrC) aerosols in northwest China, Atmospheric Chemistry and Physics, 20, 4889-4904, 10.5194/acp-20-4889-2020, 2020.
Luo, Q., Hong, J., Xu, H., Han, S., Tan, H., Wang, Q., Tao, J., Ma, N., Cheng, Y., and Su, H.: Hygroscopicity of amino acids and their effect on the water uptake of ammonium sulfate in the mixed aerosol particles, Science of the Total Environment, 734, 139318, 10.1016/j.scitotenv.2020.139318, 2020.
Morino, Y., Kondo, Y., Takegawa, N., Miyazaki, Y., Kita, K., Komazaki, Y., Fukuda, M., Miyakawa, T., Moteki, N., and Worsnop, D.: Partitioning of HNO3 and particulate nitrate over Tokyo: Effect of vertical mixing, Journal of Geophysical Research: Atmospheres, 111, 10.1029/2005JD006887, 2006.
Niu, X., Cao, J., Shen, Z., Ho, S. S. H., Tie, X., Zhao, S., Xu, H., Zhang, T., and Huang, R.: PM2.5 from the Guanzhong Plain: Chemical composition and implications for emission reductions, Atmospheric Environment, 147, 458-469, 10.1016/j.atmosenv.2016.10.029, 2016.
Okamoto, S. and Tanimoto, H.: A review of atmospheric chemistry observations at mountain sites, Progress in Earth and Planetary Science, 3, 34, 10.1186/s40645-016-0109-2, 2016.
Peng, C., Wang, Y., Wu, Z., Chen, L., Huang, R.-J., Wang, W., Wang, Z., Hu, W., Zhang, G., and Ge, M.: Tropospheric aerosol hygroscopicity in China, Atmospheric Chemistry and Physics, 20, 13877-13903, 10.5194/acp-20-13877-2020, 2020.
Petters, M. and Kreidenweis, S.: A single parameter representation of hygroscopic growth and cloud condensation nucleus activity, Atmospheric Chemistry and Physics, 7, 1961-1971, 10.5194/acp-7-1961-2007, 2007.
Pöschl, U.: Atmospheric Aerosols: Composition, Transformation, Climate and Health Effects, Angewandte Chemie International Edition, 44, 7520-7540, 10.1002/anie.200501122, 2005.
Razafindrambinina, P. N., Malek, K. A., DiMonte, K., Dawson, J. N., Raymond, T. M., Dutcher, D. D., Freedman, M. A., and Asa-Awuku, A. A.: Effects of mixing state on water-uptake properties of ammonium sulfate–Organic mixtures, Aerosol Science and Technology, 56, 1009-1021, 10.1080/02786826.2022.2114313, 2022.
Saxena, P., Hildemann, L. M., McMurry, P. H., and Seinfeld, J. H.: Organics alter hygroscopic behavior of atmospheric particles, Journal of Geophysical Research: Atmospheres, 100, 18755-18770, 10.1029/95JD01835, 1995.
Shen, M., Qi, W., Liu, Y., Zhang, Y., Dai, W., Li, L., Guo, X., Cao, Y., Jiang, Y., and Wang, Q.: Measurement report: Observational insights into the impact of dust transport on atmospheric dicarboxylic acids in ground region and free troposphere, Atmospheric Chemistry and Physics, 25, 16147-16165, 10.5194/acp-25-16147-2025, 2025.
Shen, Z., Cao, J., Arimoto, R., Zhang, R., Jie, D., Liu, S., and Zhu, C.: Chemical composition and source characterization of spring aerosol over Horqin sand land in northeastern China, Journal of Geophysical Research: Atmospheres, 112, 10.1029/2006JD007991, 2007.

https://doi.org/10.5194/egusphere-2026-6766
Preprint. Discussion started: 19 November 2026
© Author(s) 2026. CC BY 4.0 License.

Shi, J., Zhang, Z., Li, L., Liu, L., Zhou, Y., Han, S., Zhang, S., Liang, M., Xie, L., and Ran, W.: Measurement report: Hygroscopicity and mixing state of submicron aerosols in the lower free troposphere over central China: local, regional and long-range transport influences, Atmospheric Chemistry and Physics, 26, 1-13, 10.5194/acp-26-1-2026, 2026.

Sjogren, S., Gysel, M., Weingartner, E., Alfarra, M. R., Duplissy, J., Cozic, J., Crosier, J., Coe, H., and Baltensperger, U.: Hygroscopicity of the submicrometer aerosol at the high-alpine site Jungfraujoch, 3580 m a.s.l., Switzerland, Atmos. Chem. Phys., 8, 5715-5729, 10.5194/acp-8-5715-2008, 2008.

Swietlicki, E., Hansson, H.-C., Hämeri, K., Svenningsson, B., Massling, A., McFiggans, G., McMurry, P. H., Petäjä, T., Tunved, P., and Gysel, M.: Hygroscopic properties of submicrometer atmospheric aerosol particles measured with H-TDMA instruments in various environments—a review, Tellus B: Chemical and Physical Meteorology, 60, 432-469, 10.1111/j.1600-0889.2008.00350.x, 2008.

Vitali, B., Bettineschi, M., Cholakian, A., Zardi, D., Bianchi, F., Sinclair, V. A., Mikkola, J., Cristofanelli, P., Marinoni, A., and Mazzini, M.: Analysis of chemical and transport processes of biogenic aerosols over the northern Apennines: insights from the WRF-CHIMERE model, Environmental Science: Atmospheres, 4, 967-987, 10.1039/d4ea00040d, 2024.

Wang, X., Chen, Y., Guo, X., Li, J., Yang, H., and Wang, Y.: Chemical composition and hygroscopic properties of atmospheric fine particles in the tropical forest region of southwest China, Journal of Geophysical Research: Atmospheres, 131, e2025JD045358, 10.1029/2025JD045358, 2026.

Wang, X., Chen, Y., Wu, J., Li, B., Liu, Y., Zhang, Y., Cao, Y., Shen, M., Dai, W., Li, L., Guo, X., Li, J., Liu, F., and Wang, Y.: Measurement Report: Seasonal and Vertical Variations in PM2.5 Water-Soluble Matter Hygroscopicity at Mt. Hua, Central China: Insights from Inorganic and Organic Fractions, Zenodo [data set], https://doi.org/10.5281/zenodo.23855218, 2026.

Wang, Z., Wang, R., Wang, J., Wang, Y., Donahue, N. M., Tang, R., Dong, Z., Li, X., Wang, L., and Han, Y.: The seasonal variation, characteristics and secondary generation of PM2.5 in Xi'an, China, especially during pollution events, Environmental Research, 212, 113388, 10.1016/j.envres.2022.113388, 2022.

Wen, L., Yang, Y., Zhang, Y., Feng, J., Gao, R., Guo, W., Guo, S., Wang, H., Chai, F., and Herrmann, H.: Long-term variations and formation drivers of PM2.5 nitrate in a megacity of Guanzhong Plain, China: Implications for air quality management, Journal of Environmental Sciences, 166, 581-590, 10.1016/j.jes.2025.11.058, 2025.

Xue, Y., Wang, L., Jing, Y., Zhang, T., He, S., Ho, K. F., Huang, Y., Chen, L., Cui, L., and Cao, J.: Asian monsoon and local valley wind caused transport of volatile organic compounds episode across Qinling Mountain in China, Journal of Geophysical Research: Atmospheres, 128, e2022JD038256, 10.1029/2022JD038256, 2023.

Yang, S., Yang, X., Wang, Y., Wang, Z., Pang, Y., He, C., and Liu, F.: An unexpected increase in PM2.5 levels in Xi'an during the COVID-19 pandemic restrictions: The interplay of anthropogenic and natural factors, Journal of Environmental Sciences, 156, 321-331, 10.1016/j.jes.2024.07.016, 2025.

Yi, Y., Meng, J., Hou, Z., Wang, G., Zhou, R., Li, Z., Li, Y., Chen, M., Liu, X., and Li, H.: Contrasting compositions and sources of organic aerosol markers in summertime PM2.5 from urban and mountainous regions in the North China Plain, Science of The Total Environment, 766, 144187, 10.1016/j.scitotenv.2020.144187, 2021.

Zhang, T., Cao, J., Tie, X., Shen, Z., Liu, S., Ding, H., Han, Y., Wang, G., Ho, K., and Qiang, J.: Water-soluble ions in atmospheric aerosols measured in Xi'an, China: seasonal variations and sources, Atmospheric Research, 102, 110-119, 10.1016/j.atmosres.2011.06.014, 2011.

Zhang, X., Arimoto, R., An, Z., Chen, T., Zhang, G., Zhu, G., and Wang, X.: Atmospheric trace elements over source regions for Chinese dust: Concentrations, sources and atmospheric deposition on the Loess Plateau, Atmospheric Environment. Part A. General Topics, 27, 2051-2067, 10.1016/0960-1686(93)90277-6, 1993.

Zhang, Y., Yu, H., Eck, T. F., Smirnov, A., Chin, M., Remer, L. A., Bian, H., Tan, Q., Levy, R., and Holben, B. N.: Aerosol daytime variations over North and South America derived from multiyear AERONET measurements, Journal of Geophysical Research: Atmospheres, 117, 10.1029/2011JD017242, 2012.

https://doi.org/10.5194/egusphere-2026-6766
Preprint. Discussion started: 19 November 2026
© Author(s) 2026. CC BY 4.0 License.



633 Zhou, R., Afsana, S., Wei, C., and Mochida, M.: Additive water uptake of the mixtures of urban atmospheric
634 HULIS and ammonium sulfate, Journal of Geophysical Research: Atmospheres, 129, e2023JD040553,
635 10.1029/2023JD040553, 2024.
636 Zografou, O., Gini, M., Fetfatzis, P., Granakis, K., Foskinis, R., Manousakas, M. I., Tsopelas, F., Diapouli,
637 E., Dovrou, E., and Vasilakopoulou, C. N.: High-altitude aerosol chemical characterization and source
638 identification: insights from the CALISHTO campaign, Atmospheric Chemistry and Physics, 24, 8911-
639 8926, 10.5194/acp-24-8911-2024, 2024.

640

https://doi.org/10.5194/egusphere-2026-6766
Preprint. Discussion started: 19 November 2026
© Author(s) 2026. CC BY 4.0 License.

Table 1. Average concentrations (± standard deviations) of $PM_{2.5}$ chemical species at the summit and footfill sites of Mt. Hua during summer and winter.

μg m^{-3}	Summer						Winter					
	Summit			Footfill			Summit			Footfill		
	Daytime	Nighttime	Overall	Daytime	Nighttime	Overall	Daytime	Nighttime	Overall	Daytime	Nighttime	Overall
$PM_{2.5}$	11.85±6.63	9.47±5.43	10.70±6.15	37.38±14.57	25.79±12.32	31.49±14.59	33.18±30.39	30.65±22.42	31.89±26.41	153.81±79.65	123.32±67.69	138.29±74.71
WSOM	2.69±1.87	1.73±1.52	2.28±1.74	6.39±2.73	4.01±2.15	5.19±2.71	6.26±5.05	6.00±3.28	6.13±4.20	21.89±14.31	15.73±9.02	18.75±12.21
NO_3^-	0.54±0.67	0.18±0.23	0.38±0.53	3.40±2.78	2.15±2.17	2.77±2.55	4.52±5.41	4.23±3.66	4.37±4.56	17.51±15.14	14.99±10.35	15.95±12.97
SO_4^{2-}	2.13±1.29	1.57±1.15	1.91±1.22	6.22±2.74	4.24±2.13	5.22±2.63	3.64±1.93	3.14±1.52	3.38±1.74	9.48±4.94	7.57±3.13	8.51±4.19
Cl^-	0.04±0.07	0.02±0.02	0.03±0.05	0.08±0.12	0.09±0.08	0.09±0.10	0.48±0.46	0.38±0.36	0.43±0.41	3.70±1.78	3.01±1.25	3.35±1.56
NH_4^+	0.12±0.21	0.02±0.06	0.07±0.16	1.76±1.36	1.00±1.10	1.38±1.28	0.75±0.71	0.76±0.55	0.75±0.63	2.18±1.28	2.02±0.95	2.10±1.12
Na^+	0.37±0.29	0.29±0.24	0.32±0.26	0.13±0.19	0.11±0.15	0.12±0.17	0.37±0.27	0.35±0.26	0.36±0.26	0.67±0.59	0.55±0.64	0.59±0.61
K^+	0.01±0.03	0.01±0.01	0.01±0.02	0.15±0.11	0.09±0.05	0.12±0.09	0.15±0.11	0.14±0.07	0.14±0.09	0.80±0.44	0.57±0.29	0.68±0.39
Mg^{2+}	0.02±0.04	0.01±0.02	0.02±0.03	0.10±0.08	0.05±0.07	0.07±0.08	0.09±0.08	0.08±0.07	0.09±0.07	0.17±0.08	0.12±0.07	0.15±0.08
Ca^{2+}	0.15±0.20	0.10±0.12	0.13±0.17	0.61±0.54	0.39±0.39	0.49±0.48	1.20±1.29	1.09±1.21	1.14±1.24	2.94±1.35	2.05±1.38	2.49±1.42